Donor-Acceptor Ligand-to-Ligand Charge-Transfer Coordination Complexes of Nickel(II)

*Wesley W. Kramer, Lindsay A. Cameron, Ryan A. Zarkesh, Joseph W. Ziller and Alan F. Heyduk**

Department of Chemistry, University of California, Irvine, California, 92697

-- Supporting Information--

Table of Contents

Table S1. X-ray diffraction data-collection and refinement parameters for complexes **1-3**.

	(cat-tBu$_2$)Ni(bdi) **1a**	(cat-tBu$_2$)Ni(adi) **1b**	(cat-tBu$_2$)Ni(pdi) **1c**	(cat-Cl$_4$)Ni(bdi) **2a**	(cat-Cl$_4$)Ni(adi) **2b**	(cat-Cl$_4$)Ni(pdi) **2c**	(pdiol)Ni(bdi) **3a**	(pdiol)Ni(adi) **3b**	(pdiol)Ni(pdi) **3c**
empirical formula	$C_{43}H_{56}N_2O_{42}Ni$	$C_{44}H_{53}N_2O_2Ni$•($C_4H_{10}O)_{0.5}$	$C_{46}H_{50}N_2O_2Ni$	$C_{28}H_{28}N_2O_2Cl_4Ni$•($CHCl_3$)	$C_{36}H_{28}Cl_4N_2O_2Ni$•(C_4H_8O)	$C_{38}H_{30}Cl_4N_2O_2Ni$•$(CH_2Cl_2)_2$	$C_{36}H_{36}N_2O_2Ni$	$C_{44}H_{36}N_2O_2$ Ni	$C_{46}H_{38}N_2O_2Ni$ • ¼(C_6H_6)
formula weight	691.61	732.61	721.59	744.40	793.22	917.00	587.38	683.46	729.02
crystal system	Monoclinic	Orthorombic	Monoclinic	Monoclinic	Monoclinic	Monoclinic	Monoclinic	Monoclinic	Triclinic
space group	$P2_1/c$	$Pbca$	$P2_1/n$	$P2_1/n$	$P2_1/c$	$P2_1/n$	$P2_1/n$	$C2/c$	$P\bar{1}$
a/ Å	17.2738(6)	11.4199(4)	13.8202(10)	11.2584(5)	12.4095(8)	13.6879(8)	11.5185(7)	17.5572(17)	11.7093(6)
b/ Å	15.88175(6)	26.3839(8)	20.1252915)	24.1938(11)	17.2423(12)	19.9176(12)	14.8995(9)	23.260(2)	19.2228(10)
c/ Å	14.84	26.4205(8)	14.9286(11)	11.755895)	17.1607(12)	15.1290(9)	17.7806(10)	8.5639(8)	20.4554(11)
α/deg	90.00	90.00	90.00	90.00	90.00	90.00	90.00	90.00	105.1048(7)
β/deg	102.377(4)	90.00	114.2540(9)	98.9900(10)	103.4560(10)	104.2724(7)	91.4097(7)	109.2445(12)	103.0242(7)
γ/deg	90.00	90.00	90.00	90.00	90.00	90.00	90.00	90.00	107.2972(7)
V /Å^3	3960.0(2)	7960.50	3785.7(5)	3162.792)	3571.0(4)	3997.3(4)	3050.6(3)	3301.9(5)	4008.5(4)
Z	4.00	8.00	4.00	4.00	4.00	4.00	4.00	4.00	4.00
refl collected	47072	69004	43139	37758	30506	45818	33246.00	18153.00	49543.00
indep refl	9839	10048	8937	7853	8301	9470	6725	4182.00	19320.00
R_1	0.0408	0.0393	0.0429	0.0240	0.0287	0.0367	0.05	0.04	0.04
wR_2	0.11	0.11	0.11	0.06	0.08	0.09	0.11	0.10	0.10

Electrochemical analysis of complexes 1-3.
Electrochemical data were collected at 298 K in THF solutions that were 1.0 mM in analyte and 0.1 M in $[Bu_4N][PF_6]$ electrolyte using a glassy-carbon working electrode. All potentials were referenced to $[Cp_2Fe]^{+/0}$ using an internal standard.

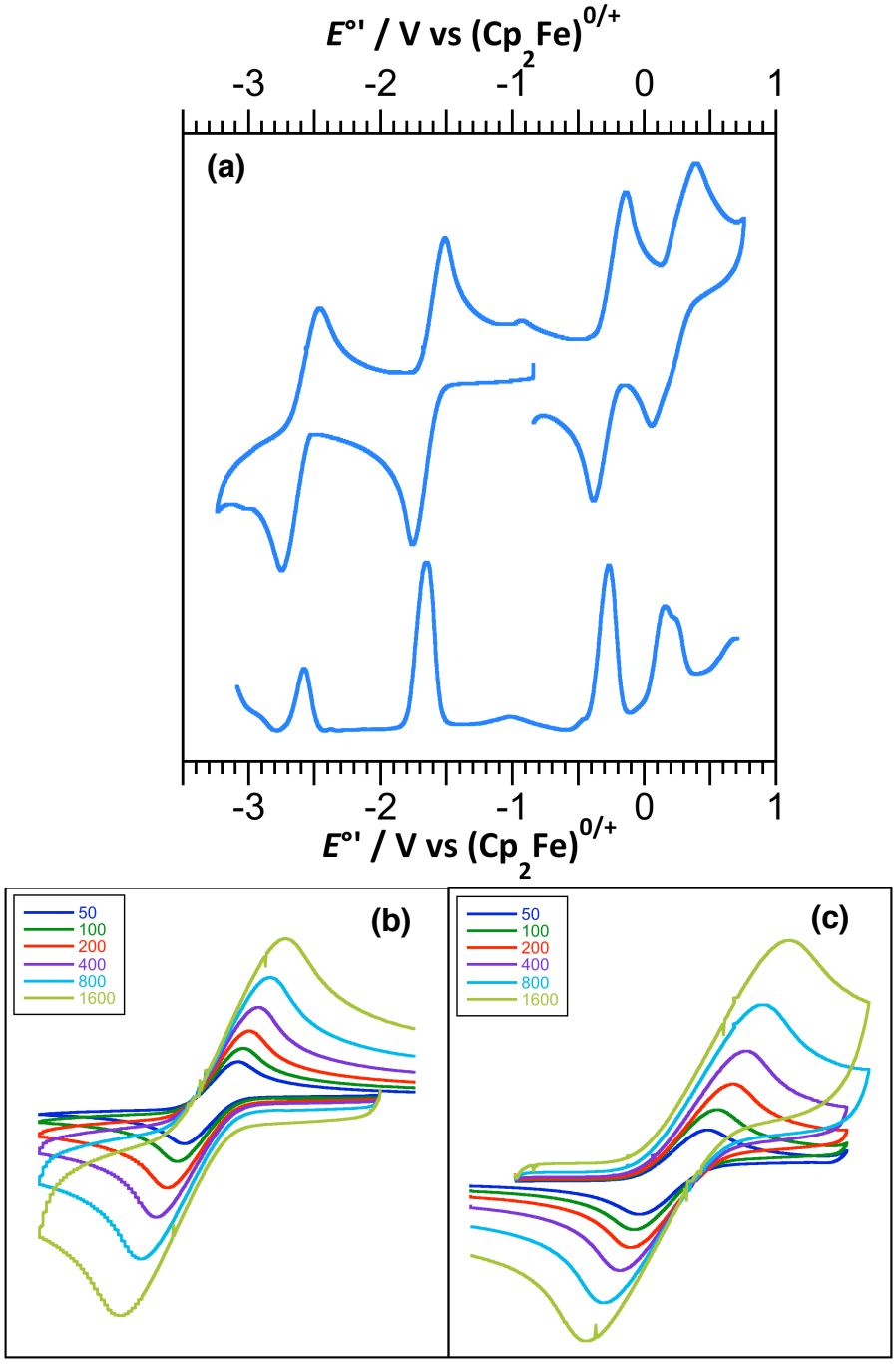

Figure S1. (a) Cyclic voltammogram and differential pulse voltammogram for (cat-*t*Bu$_2$)Ni(bdi) (**1a**) in THF, (b) scan-rate dependence of the first reduction ($E_3°'$) of **1a**, and (c) scan-rate dependence of the first oxidation ($E_2°'$) of **1a**.

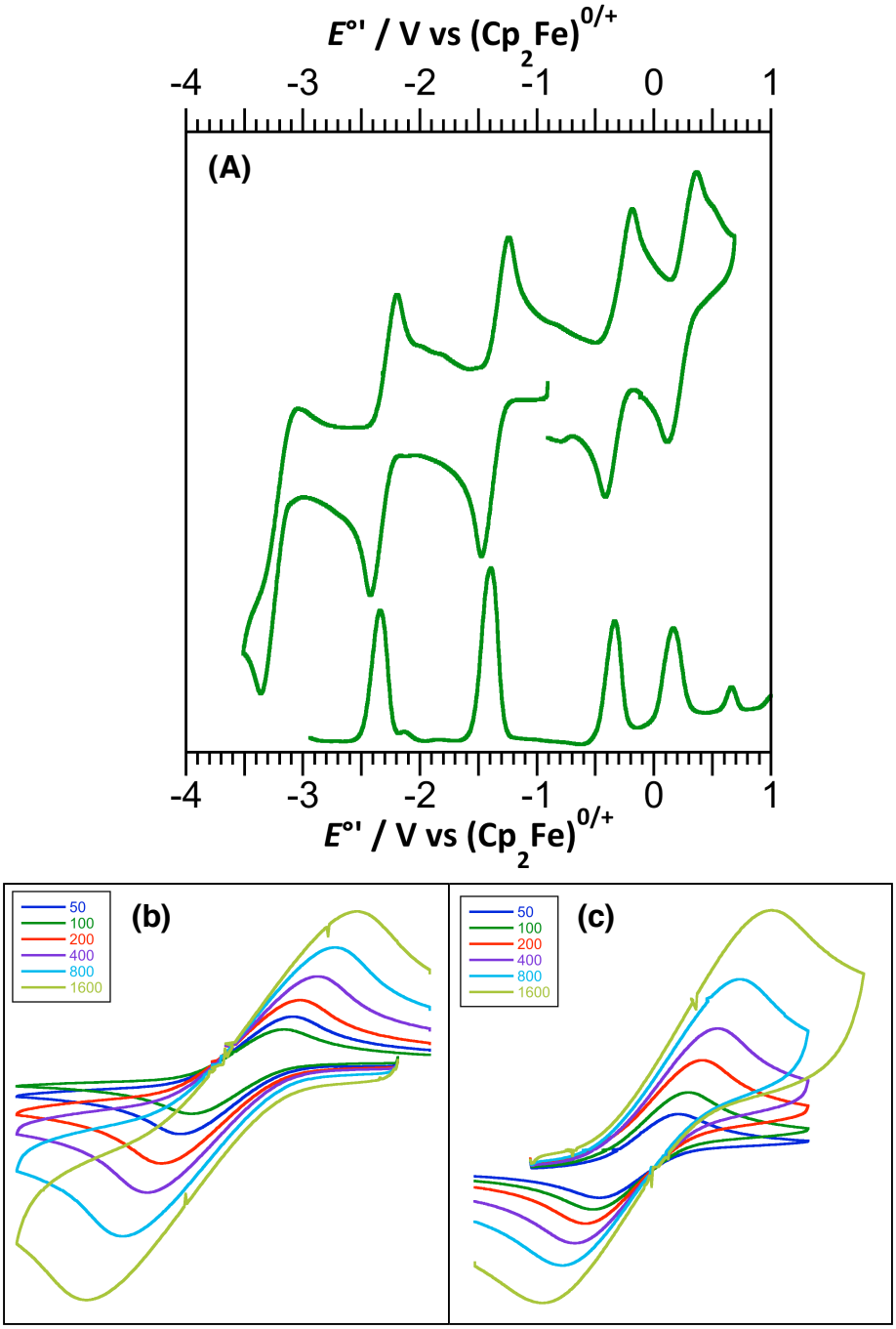

Figure S2. (a) Cyclic voltammogram and differential pulse voltammogram for (cat-*t*Bu$_2$)Ni(adi) (**1b**) in THF, (b) scan-rate dependence of the first reduction ($E_3°'$) of **1b**, and (c) scan-rate dependence of the first oxidation ($E_2°'$) of **1b**.

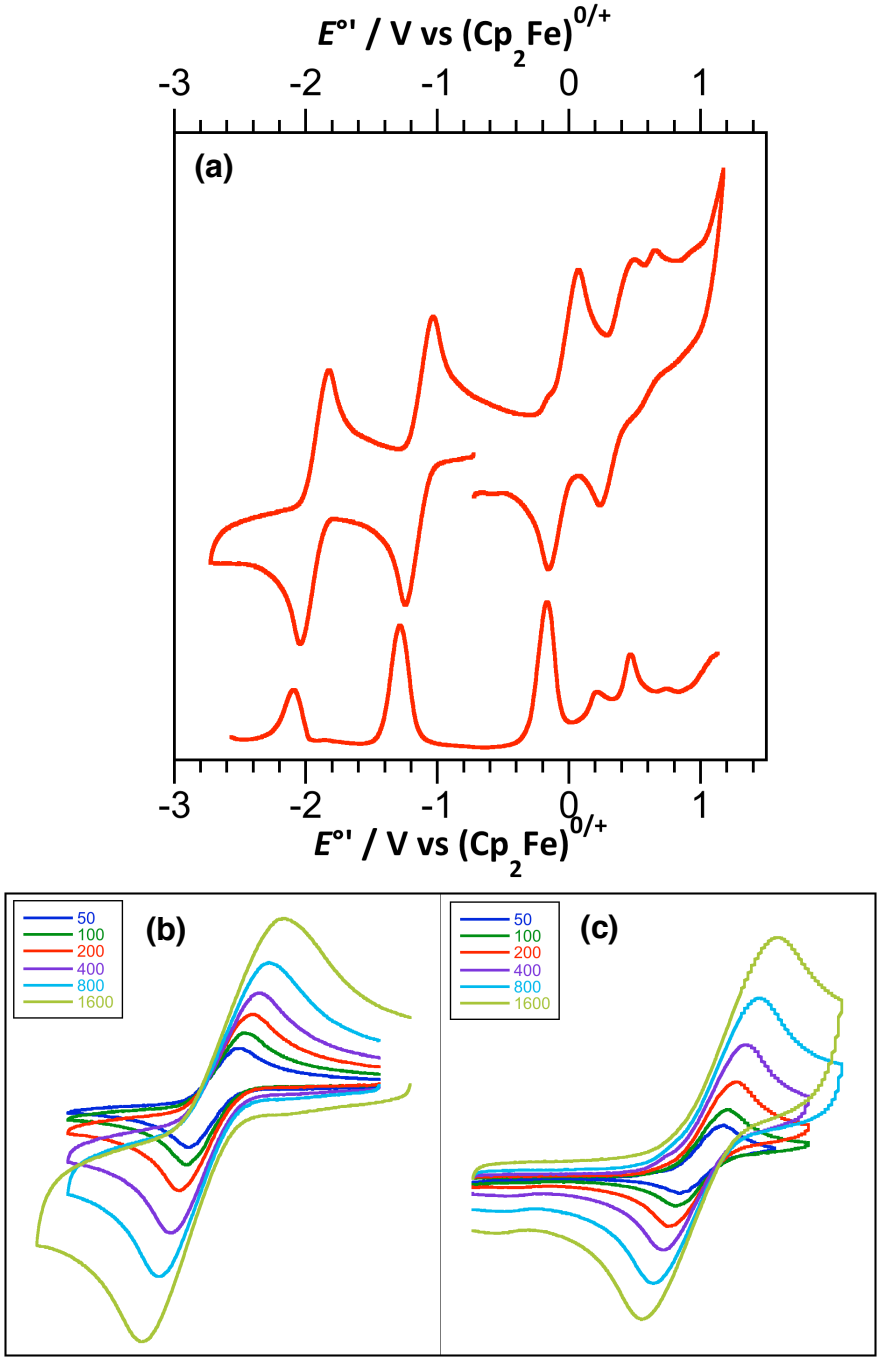

Figure S3. (a) Cyclic voltammogram and differential pulse voltammogram for (cat-*t*Bu$_2$)Ni(pdi) (**1c**) in THF, (b) scan-rate dependence of the first reduction ($E_3°'$) of **1c**, and (c) scan-rate dependence of the first oxidation ($E_2°'$) of **1c**.

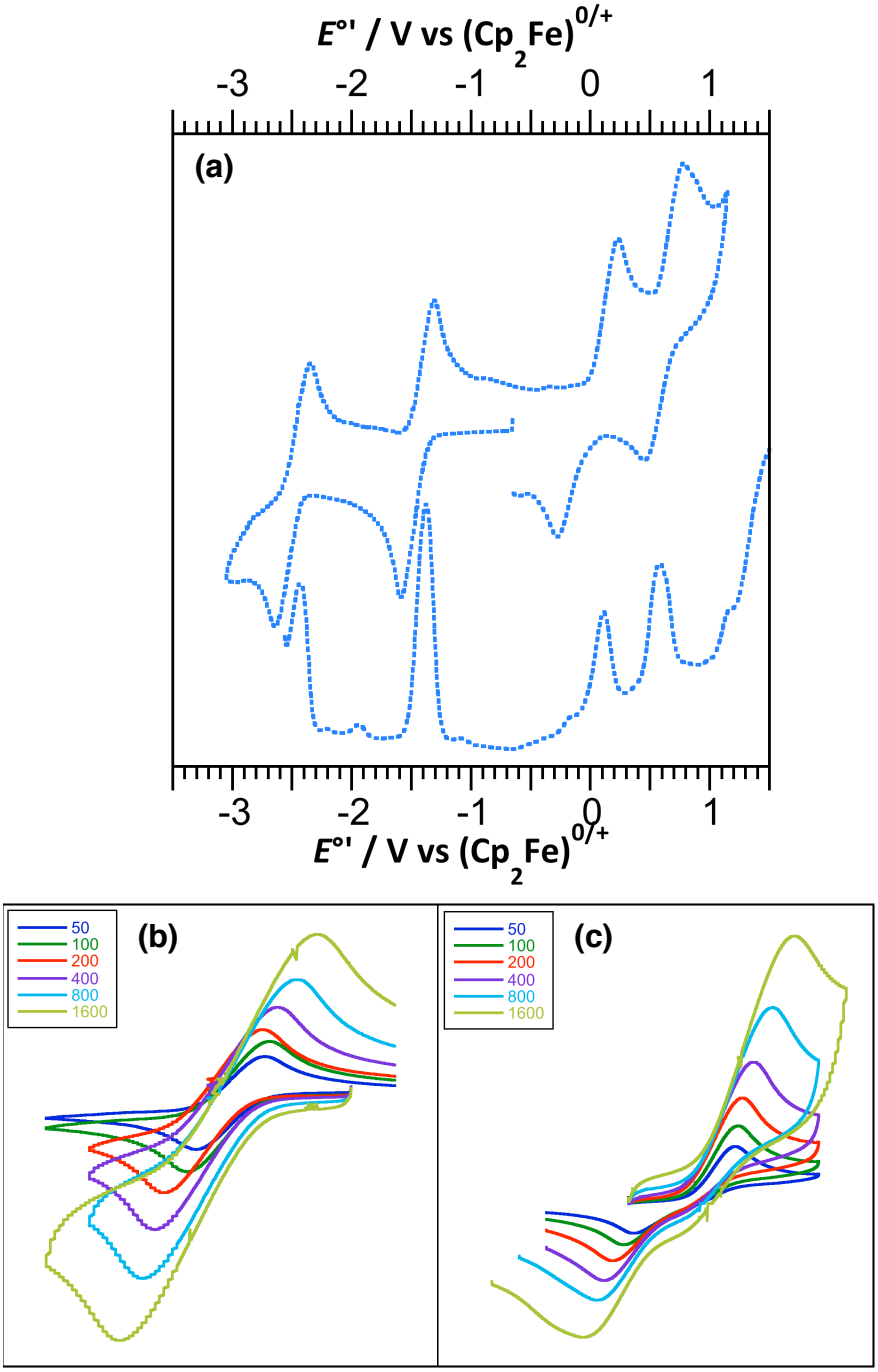

Figure S4. (a) Cyclic voltammogram and differential pulse voltammogram for ($catCl_4$)Ni(bdi) (**2a**) in THF, (b) scan-rate dependence of the first reduction ($E_3°'$) of **2a**, and (c) scan-rate dependence of the first oxidation ($E_2°'$) of **2a**.

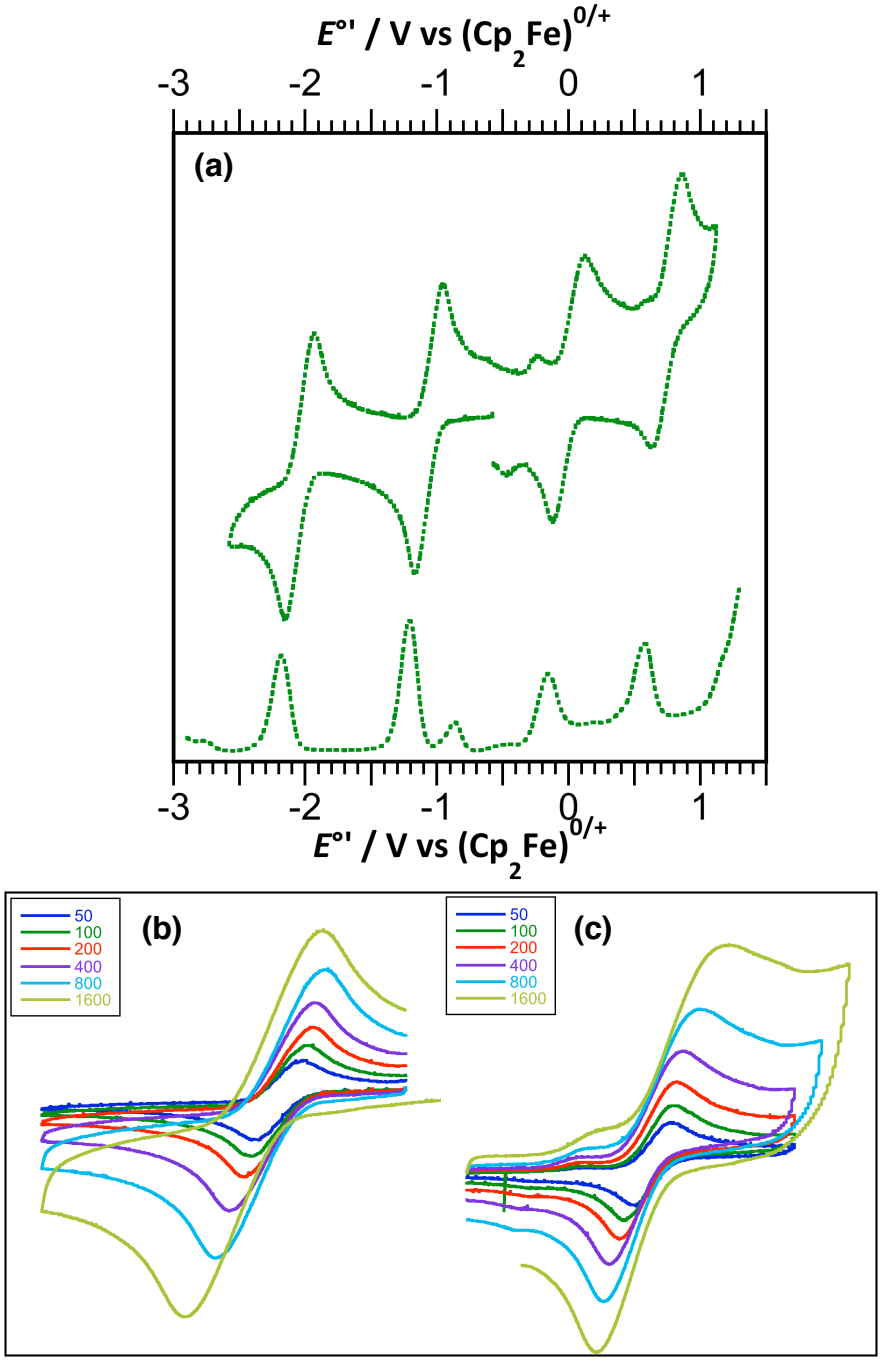

Figure S5. (a) Cyclic voltammogram and differential pulse voltammogram for ($catCl_4$)Ni(adi) (**2b**) in THF, (b) scan-rate dependence of the first reduction ($E_3°'$) of **2b**, and (c) scan-rate dependence of the first oxidation ($E_2°'$) of **2b**.

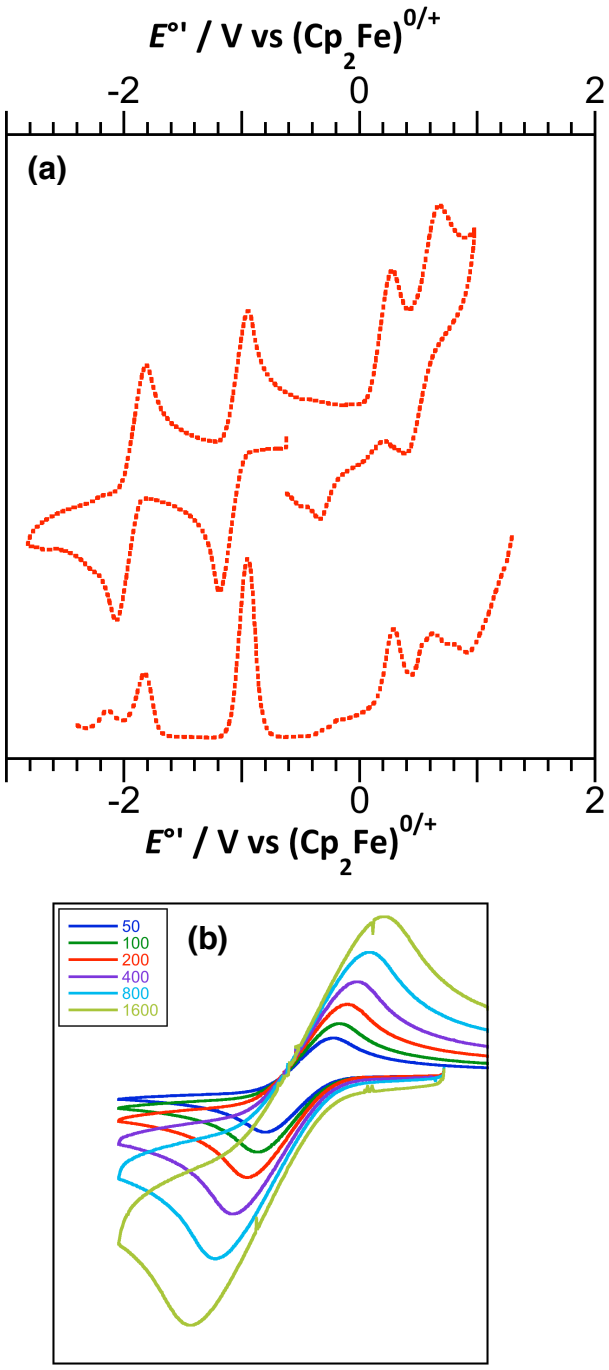

Figure S6. (a) Cyclic voltammogram and differential pulse voltammogram for ($catCl_4$)Ni(pdi) (**2c**) in THF and (b) scan-rate dependence of the first reduction ($E_3°'$) of **2c**.

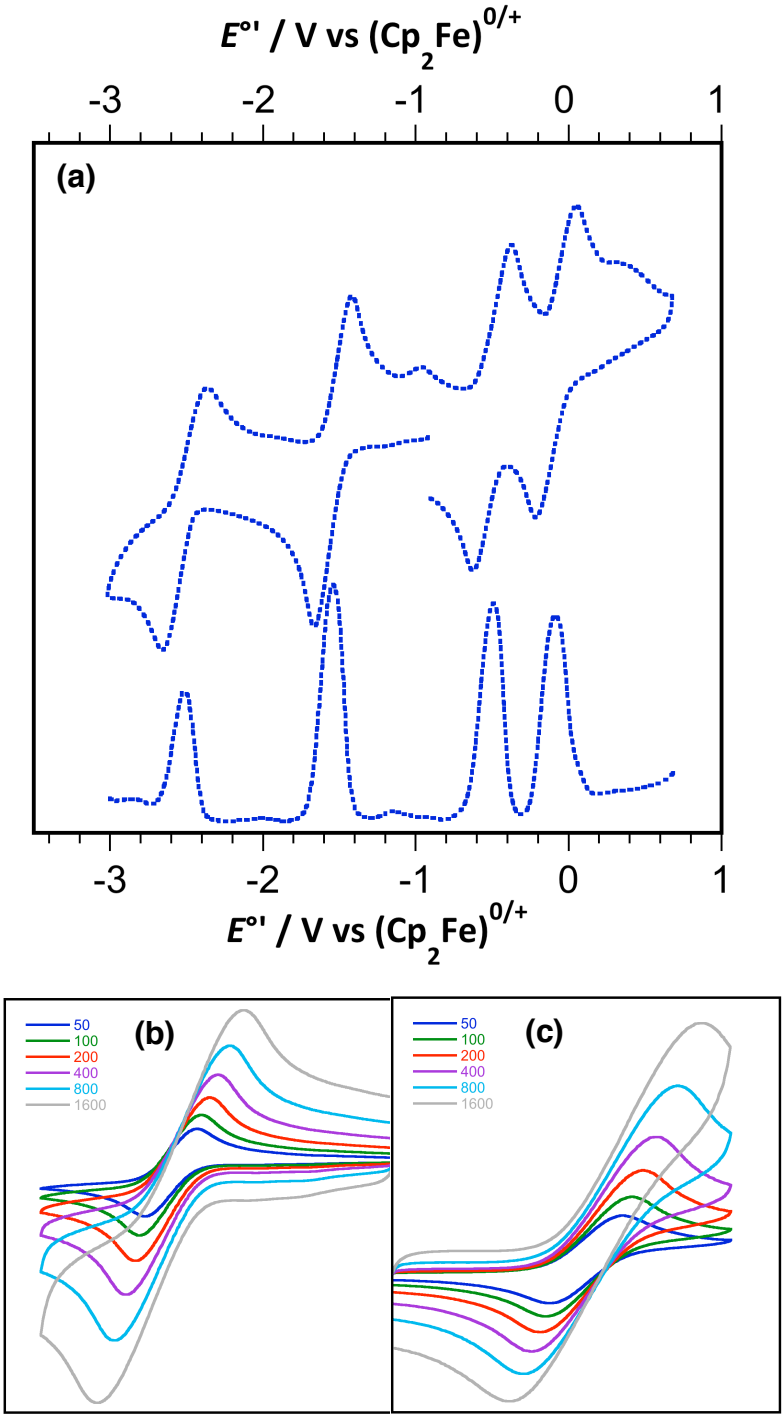

Figure S7. (a) Cyclic voltammogram and differential pulse voltammogram for (pdiol)Ni(bdi) (**3a**) in THF, (b) scan-rate dependence of the first reduction ($E_3°'$) of **3a** and (c) scan-rate dependence of the first oxidation ($E_2°'$) of **3a**.

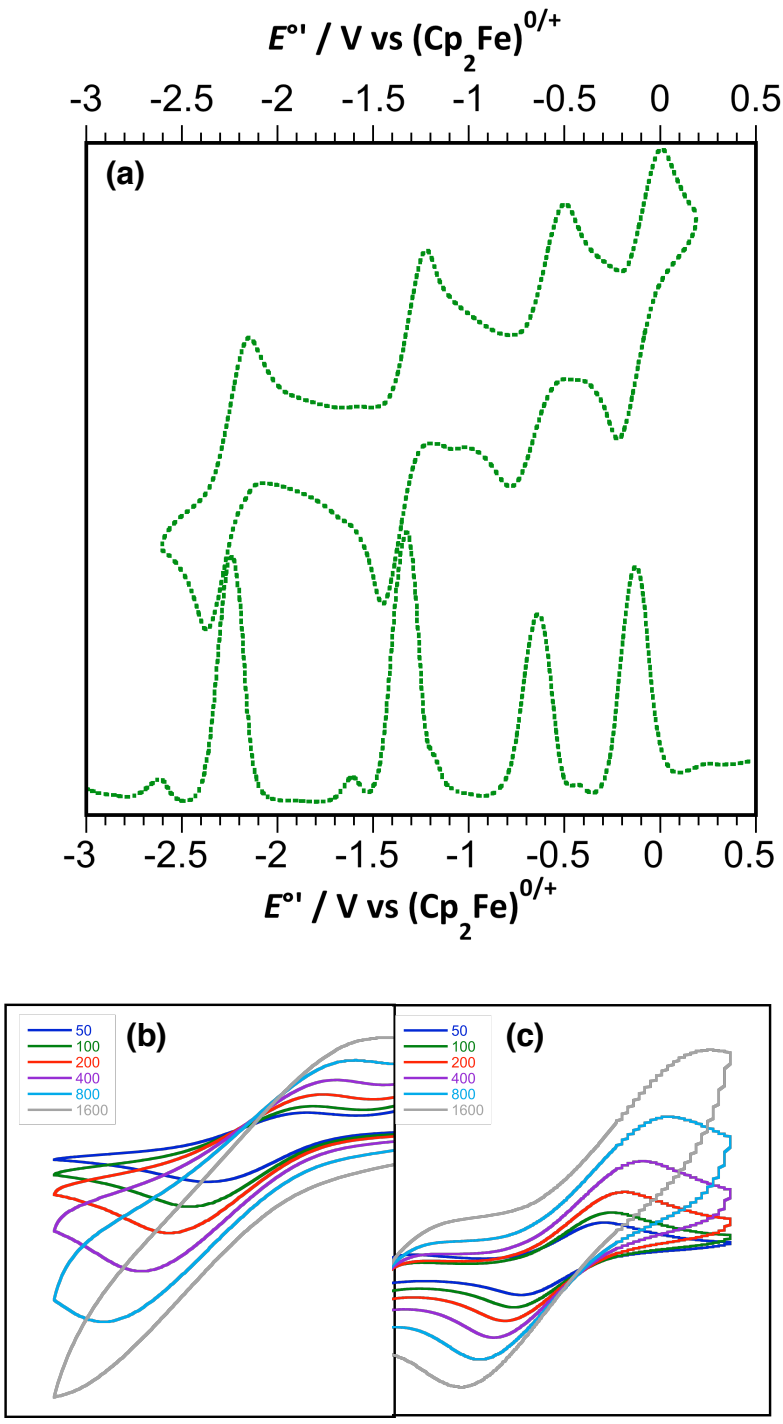

Figure S8. (a) Cyclic voltammogram and differential pulse voltammogram for (pdiol)Ni(adi) (**3b**) in THF, (b) scan-rate dependence of the first reduction ($E_3°'$) of **3b**, and (c) scan-rate dependence of the first oxidation ($E_2°'$) of **3b**.

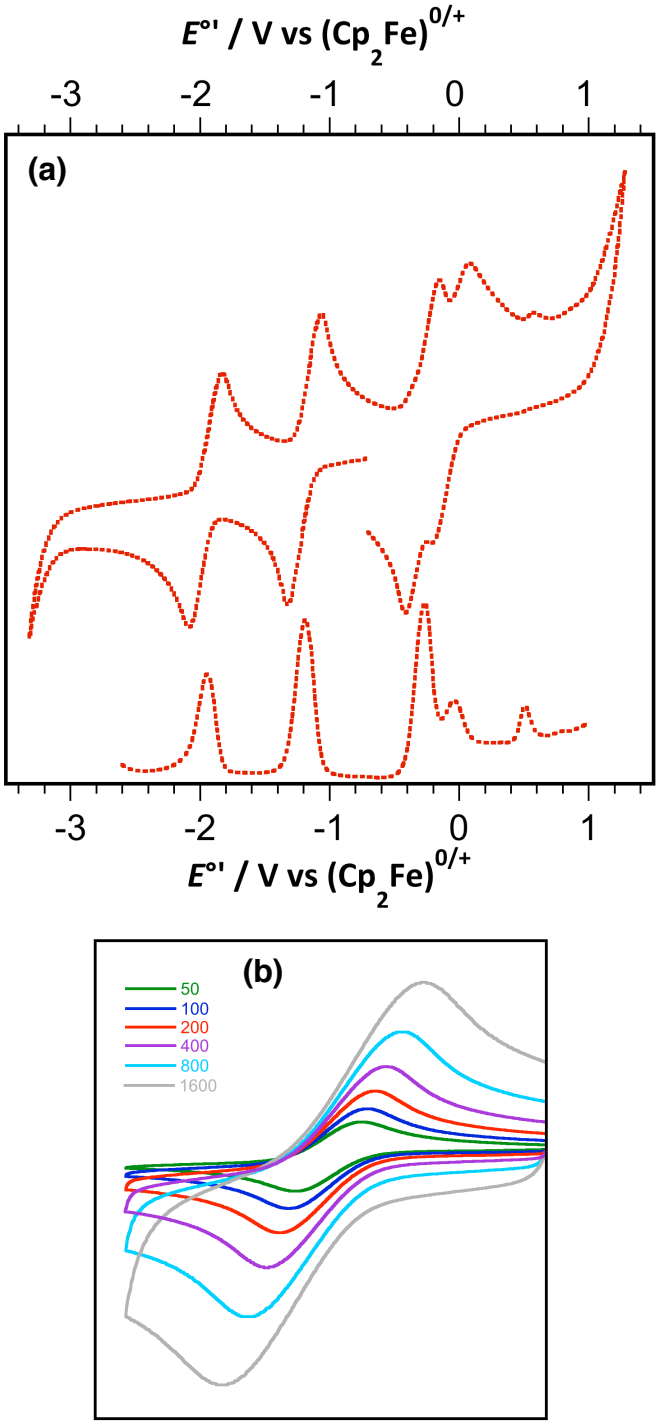

Figure S9. (a) Cyclic voltammogram and differential pulse voltammogram for (pdiol)Ni(pdi) (**3c**) in THF and (b) scan-rate dependence of the first reduction ($E_3°'$) of **3c**.

Solvatochromic data for Complexes 1-3.

In order to eliminate systematic errors to the excited state energy arising from changes in the intensity of different vibronic transitions, the energy of an excited state in a given solvent was determined from the low-energy onset of the LL'CT transition as shown in Figure S10.

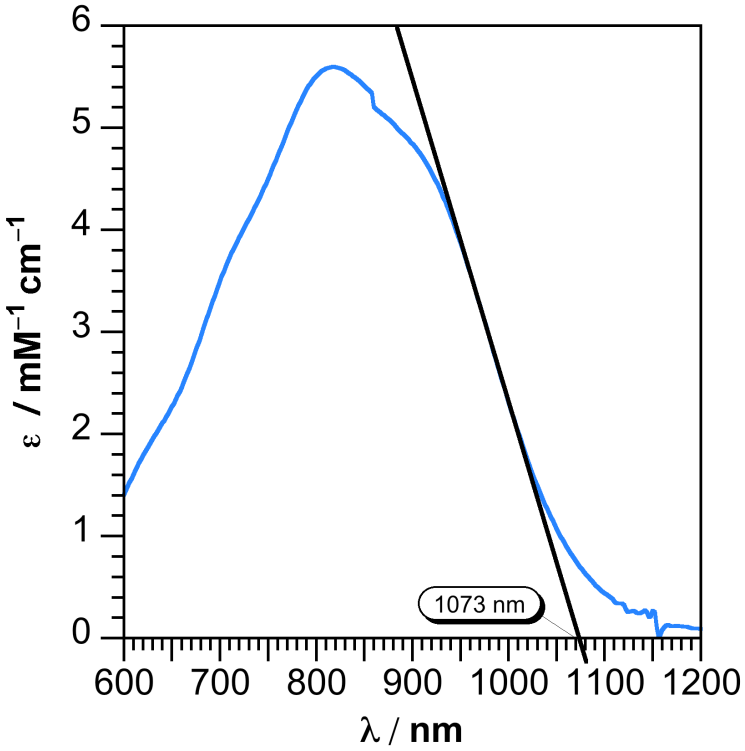

Figure S10. Estimated low-energy onset of the LL'CT transition for complex **1a** in CH_2Cl_2.

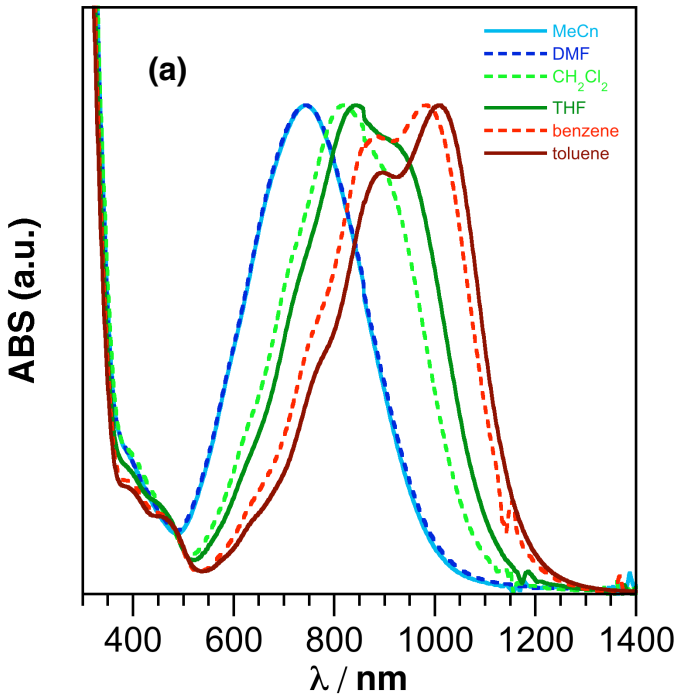

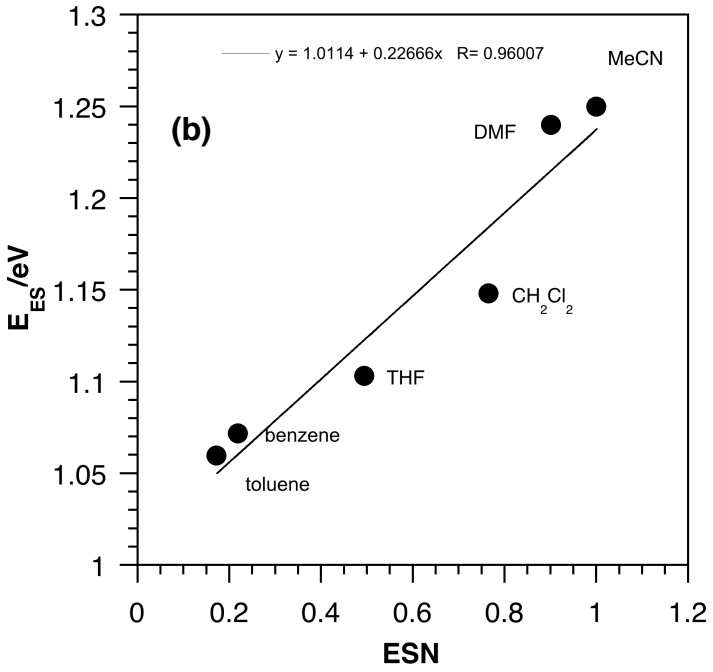

Figure S11. (a) Absorption spectra of (cat-tBu_2)Ni(bdi) (**1a**) in toluene (maroon), benzene (red), THF (green), CH_2Cl_2 (light green), DMF (blue) and MeCN (light blue) at 25 °C. (b) Plot of the estimated excited state energy in eV vs the empirical solvent number (*J Am Chem Soc* **1996**, *118*, 1949–1960).

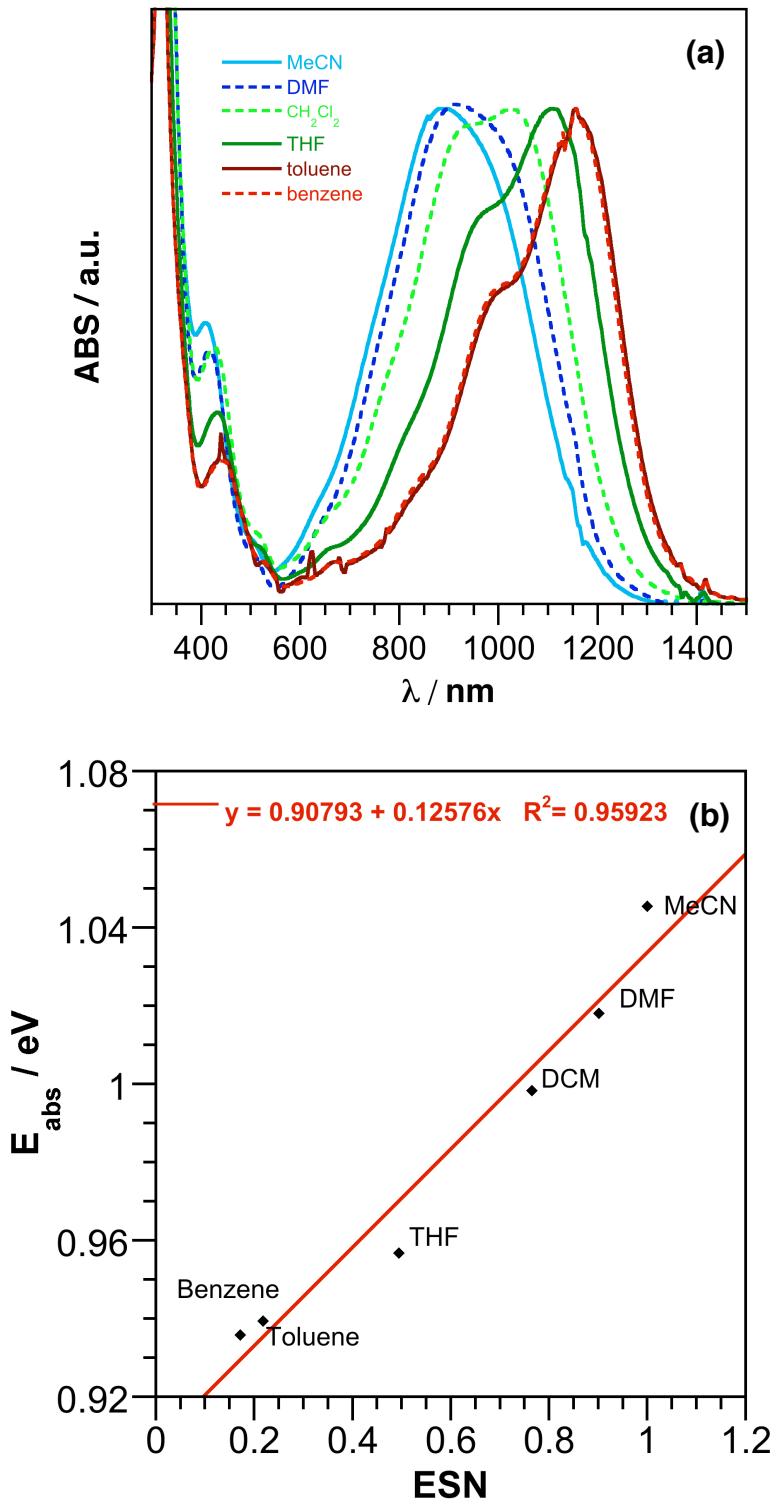

Figure S12. (a) Absorption spectra of (cat-tBu$_2$)Ni(adi) (**1b**) in toluene (maroon), benzene (red), THF (green), CH_2Cl_2 (light green), DMF (blue) and MeCN (light blue) at 25 °C. (b) Plot of the estimated excited state energy in eV vs the empirical solvent number (*J Am Chem Soc* **1996**, *118*, 1949–1960).

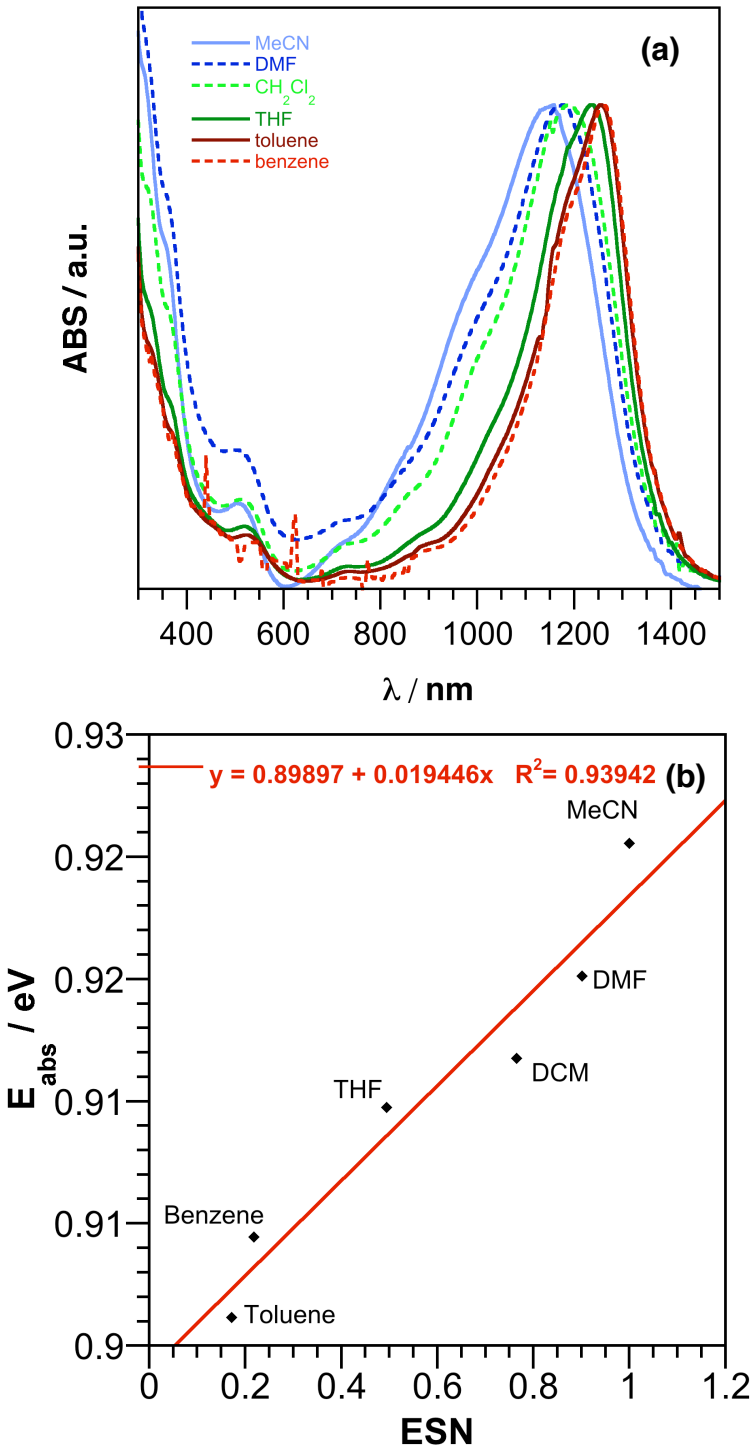

Figure S13. (a) Absorption spectra of (cat-tBu$_2$)Ni(bdi) (**1c**) in toluene (maroon), benzene (red), THF (green), CH_2Cl_2 (light green), DMF (blue) and MeCN (light blue) at 25 °C. (b) Plot of the estimated excited state energy in eV vs the empirical solvent number (*J Am Chem Soc* **1996**, *118*, 1949–1960).

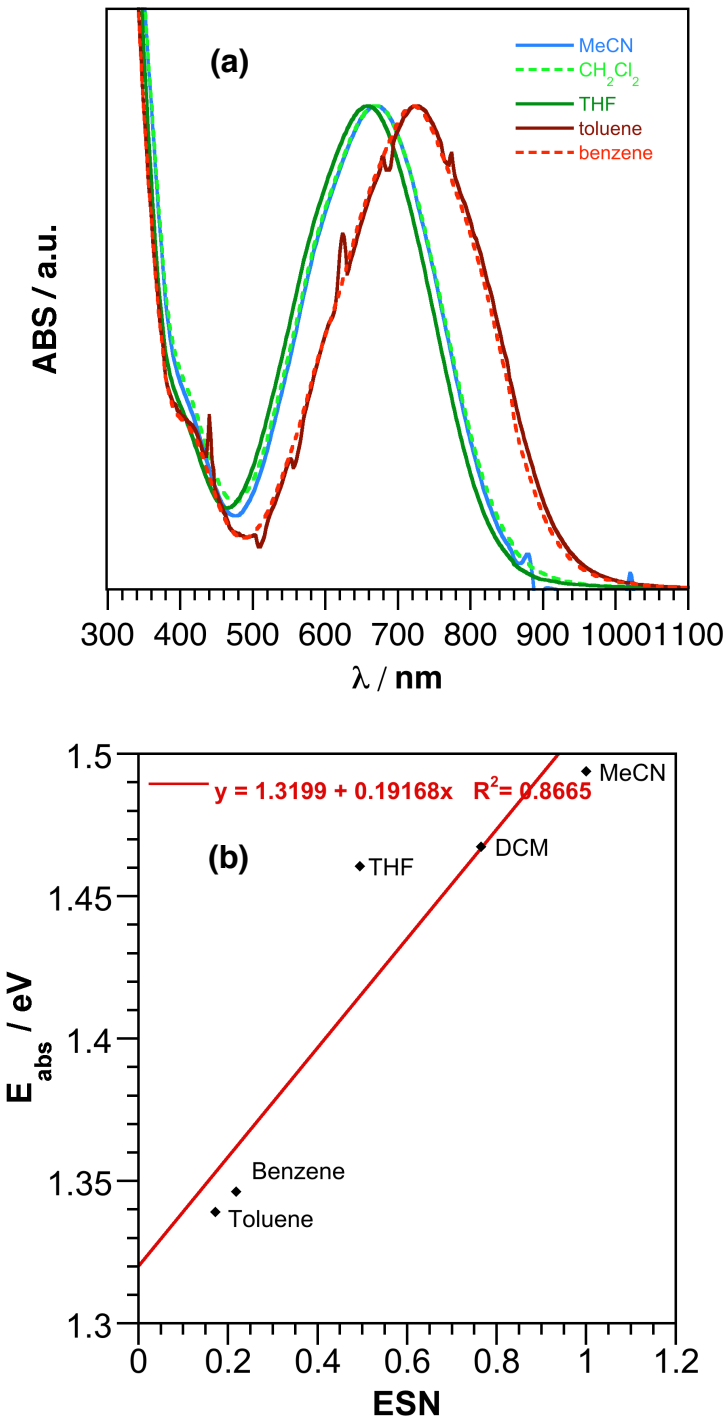

Figure S14. (a) Absorption spectra of ($catCl_4$)Ni(bdi) (**2a**) in toluene (maroon), benzene (red), THF (green), CH_2Cl_2 (light green) and MeCN (light blue) at 25 °C. (b) Plot of the estimated excited state energy in eV vs the empirical solvent number (*J Am Chem Soc* **1996**, *118*, 1949–1960).

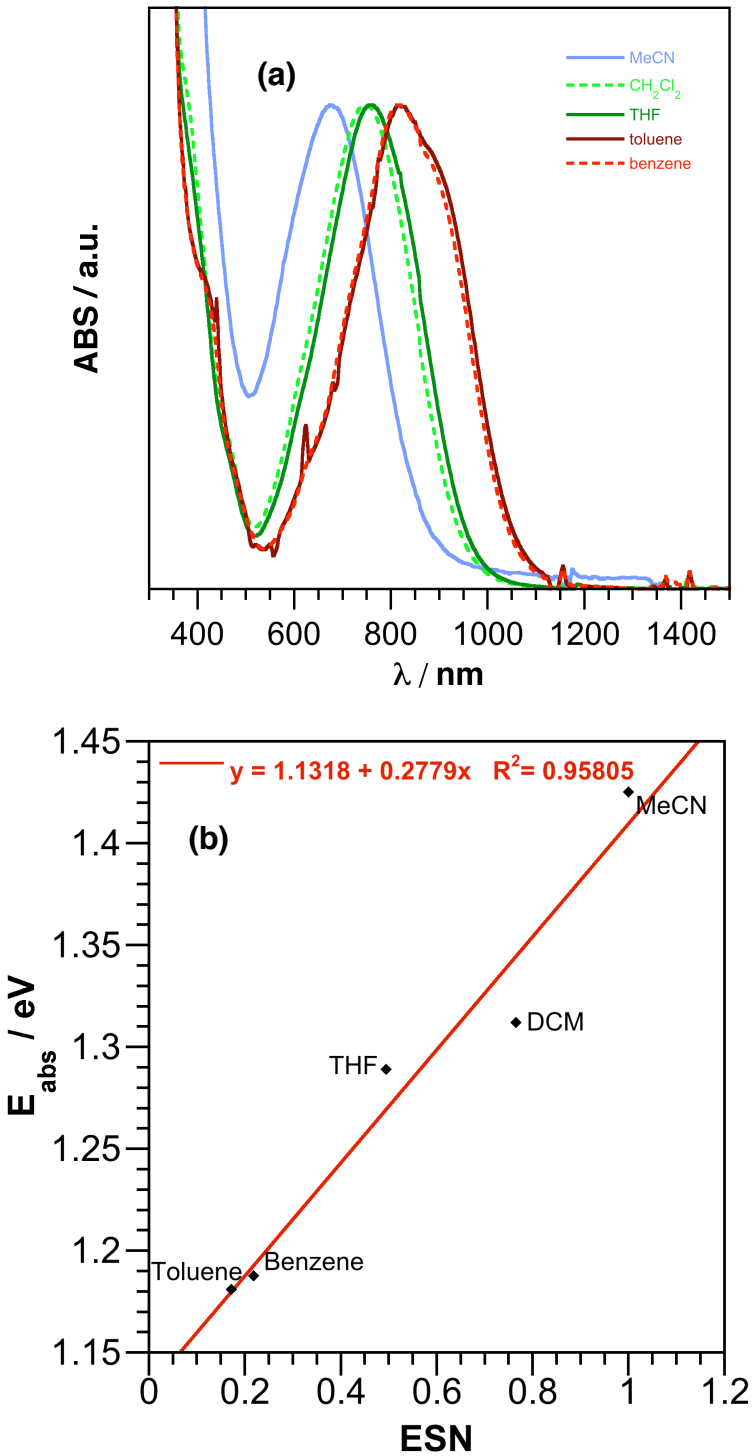

Figure S15. (a) Absorption spectra of ($catCl_4$)Ni(adi) (**2b**) in toluene (maroon), benzene (red), THF (green), CH_2Cl_2 (light green) and MeCN (light blue) at 25 °C. (b) Plot of the estimated excited state energy in eV vs the empirical solvent number (*J Am Chem Soc* **1996**, *118*, 1949–1960).

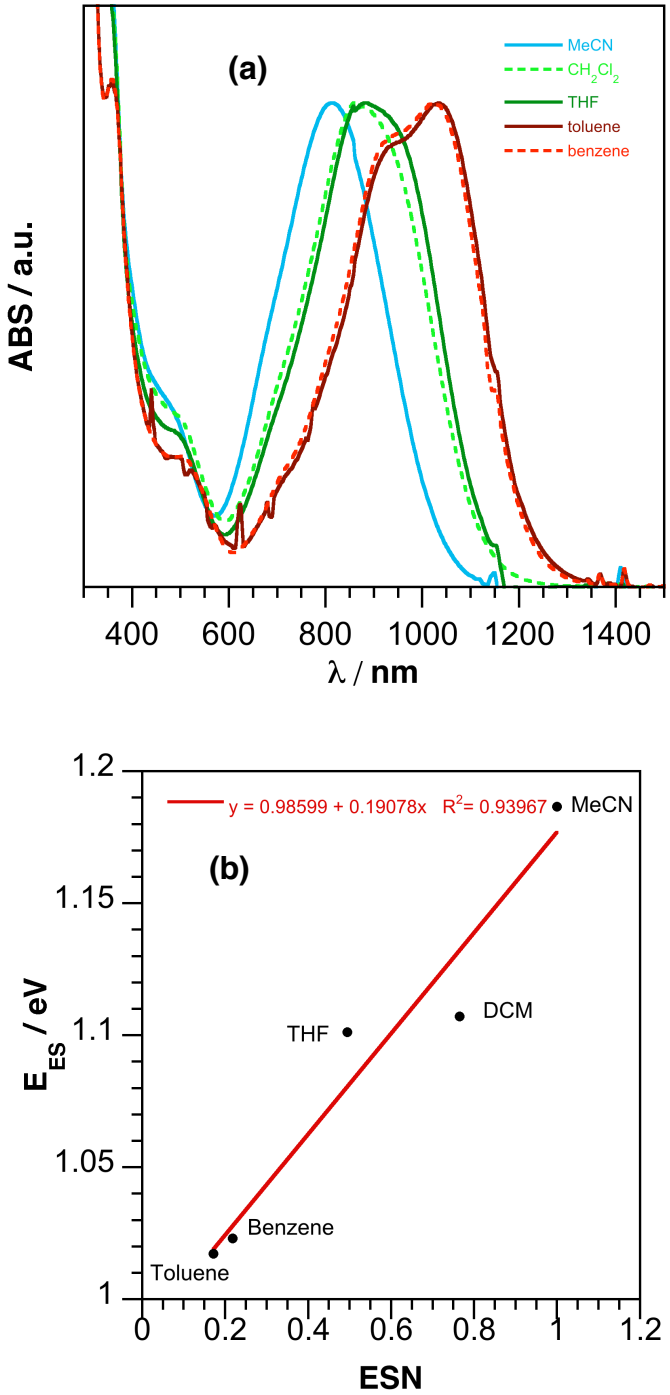

Figure S16. (a) Absorption spectra of ($catCl_4$)Ni(pdi) (**2c**) in toluene (maroon), benzene (red), THF (green), CH_2Cl_2 (light green), and MeCN (light blue) at 25 °C. (b) Plot of the estimated excited state energy in eV vs the empirical solvent number (*J Am Chem Soc* **1996**, *118*, 1949–1960).

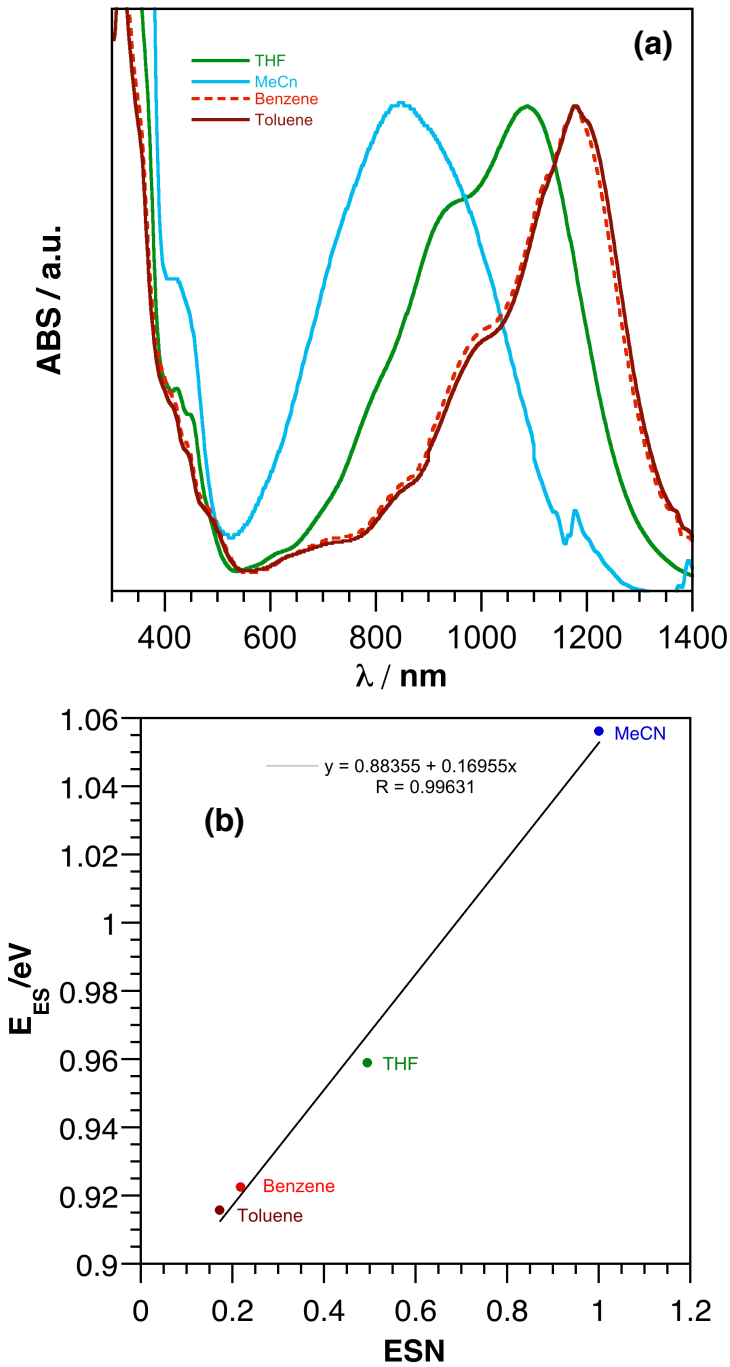

Figure S17. (a) Absorption spectra of (pdiol)Ni(bdi) (**3a**) in toluene (maroon), benzene (red), THF (green), and MeCN (light blue) at 25 °C. (b) Plot of the estimated excited state energy in eV vs the empirical solvent number (*J Am Chem Soc* **1996**, *118*, 1949–1960).

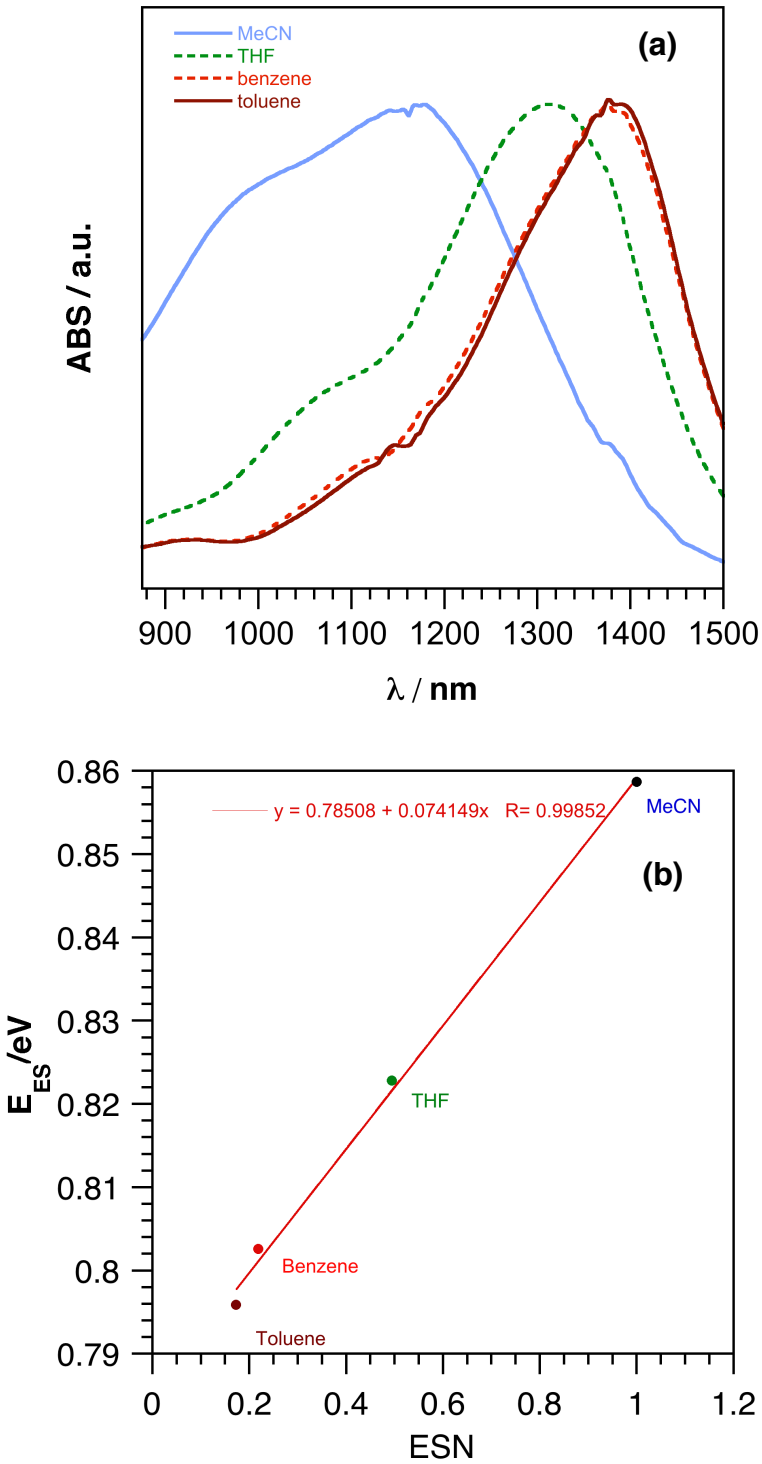

Figure S18. (a) Absorption spectra of (pdiol)Ni(adi) (**3b**) in toluene (maroon), benzene (red), THF (green), and MeCN (light blue) at 25 °C. (b) Plot of the estimated excited state energy in eV vs the empirical solvent number (*J Am Chem Soc* **1996**, *118*, 1949–1960).

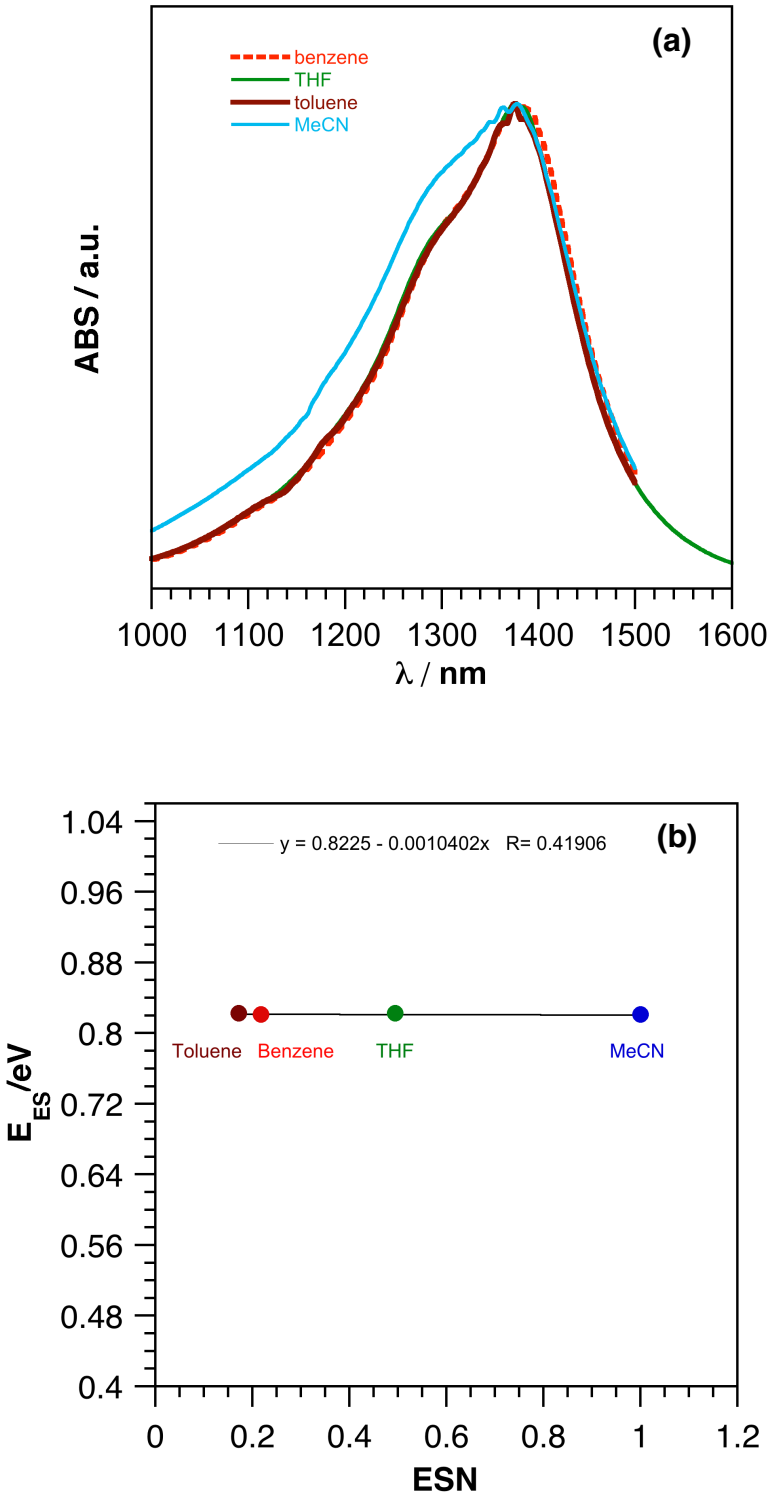

Figure S19. (a) Absorption spectra of (pdiol)Ni(pdi) (**3c**) in toluene (maroon), benzene (red), THF (green), and MeCN (light blue) at 25 °C. (b) Plot of the estimated excited state energy in eV vs the empirical solvent number (*J Am Chem Soc* **1996**, *118*, 1949–1960).